The Astrophysical Journal, 635:L189–L192, 2005 December 20

A NEW VARIETY OF CORONAL MASS EJECTION: STREAMER PUFFS FROM COMPACT EJECTIVE FLARES

A. Bemporad
Dipartimento di Astronomia e Scienza dello Spazio, Università degli Studi di Firenze, Largo Enrico Fermi 2, I-50125 Florence, Italy
Alphonse C. Sterling and Ronald L. Moore
Space Science Branch, XD12, NASA Marshall Space Flight Center, Huntsville, AL 35805
and
G. Poletto
Osservatorio Astrofisico di Arcetri, INAF, Largo E. Fermi 5, I-50125 Florence, Italy
Received 2005 September 5; accepted 2005 November 15; published 2005 December 6

ABSTRACT

We report on *SOHO* UVCS, LASCO, EIT, and MDI observations of a series of narrow ejections that occurred at the solar limb. These ejections originated from homologous compact flares whose source was an island of included polarity located just inside the base of a coronal streamer. Some of these ejections result in narrow CMEs ("streamer puffs") that move out along the streamer. These streamer puffs differ from "streamer blowout" CMEs in that (1) while the streamer is transiently inflated by the puff, it is not disrupted, and (2) each puff comes from a compact explosion in the outskirts of the streamer arcade, not from an extensive eruption along the main neutral line of the streamer arcade. From the observations, we infer that each streamer puff is produced by means of the inflation or blowing open of an outer loop of the arcade by ejecta from the compact-flare explosion in the foot of the loop. So, in terms of their production, our streamer puffs are a new variety of CME.

Subject headings: Sun: coronal mass ejections (CMEs) — Sun: magnetic fields — Sun: UV radiation

1. INTRODUCTION

While the more obvious coronal mass ejections (CMEs) have widths of 30°–90° (see, e.g., St. Cyr et al. 1999, 2000), recent space-based observations from LASCO (the Large Angle Spectroscopic Coronagraph; Brueckner et al. 1995) on board *SOHO* (the *Solar and Heliospheric Observatory*) also show "narrow CMEs," with angular widths of about 15° or less (Gilbert et al. 2001; Dobrzycka et al. 2003). Here we report on a series of rather narrow CMEs observed in a streamer. We call these disturbances "streamer puffs" from their morphology in LASCO images. In LASCO, they appear as a plasmoid or as a gust of solar wind that moves out along the streamer, transiently inflating the streamer but leaving it intact. Observations at lower heights by EIT (the Extreme Ultraviolet Imaging Telescope; Delaboudinière et al. 1995) show that they arise from homologous compact ejective flare events at an outer footpoint of the magnetic arcade under the streamer. The ejected plasma crosses the UVCS (Ultraviolet Coronagraph Spectrometer; Kohl et al. 1995) slit at 1.7 $R_\odot$; in correspondence with these events, UVCS spectra show many brightenings in the C III λ977 and O VI λλ 1032, 1037 spectral lines. Full-disk magnetograms from the *SOHO* MDI (Michelson Doppler Imager; Scherrer et al. 1995) show the magnetic flux arrangement at the base of the streamer and the magnetic setting of the compact flares and are key to our scenario for producing the puffs. We infer that in each episode magnetoplasma from the footpoint eruption shoots up along a high magnetic loop of the arcade and explodes or expands the loop top, causing it to become or to emit the streamer puff. These narrow CMEs differ from streamer blowout CMEs in that they do not destroy the streamer in which they occur, and in that they result from compact-flare explosions seated in the flank of the streamer arcade rather than from an eruption seated on the main neutral line of the streamer arcade.

2. OBSERVATIONS

We discovered our streamer-puff events from a 2.3 day observing run with UVCS starting late on 2002 November 26, when there was a large streamer on the northwest limb. We found corresponding events in LASCO coronal movies and in EIT movies of the low solar atmosphere at the base of the streamer. During the first half of the UVCS run, EIT's high-cadence (12 minute) observations were from its He II 304 Å filter (lasting until 00:48 UT on the 28th), which detects upper chromosphere and transition region plasma at around 6×10^4 K. For the rest of the UVCS run, EIT's 12 minute cadence observations were from its Fe XII 195 Å filter, which observes the low corona at around 1.5×10^6 K. At the foot of the south side of the streamer, the He II movies show several homologous compact ejective flares that occurred in synchrony with UVCS C III brightenings with or without LASCO streamer puffs. Similar UVCS C III brightenings and LASCO streamer puffs occurred during the EIT Fe XII interval, but the compact eruptions at the base of the streamer are much less visible in the Fe XII movies than in the He II movies.

Figure 1*a* shows the active region (NOAA AR 10197) near the west limb that is the source of the recurring eruptions, with the white circle showing the compact mixed-polarity region from which the eruptions originate. This compact region is at the north edge of a positive-polarity sunspot. The black outside the circle on the limbward side of this sunspot is actually an area of positive polarity; it appears negative because of line-of-sight projection of the nearly horizontal penumbral field. Earlier magnetograms (e.g., that for 2002 November 21) indicate that the location of the circle is a true negative-polarity feature at the northern edge of the positive spot, surrounded by weaker positive flux. That is, the circled negative feature is embedded in a sea of positive polarity. Figures 1*b*–1*c* show an example of a puff-producing eruption in He II: within the compact-flare area (He II brightening on the active region; Fig. 1*b*), an ejection appears emanating and being expelled from near the location of the mixed polarity of Figure 1*a*. Figure 1*e* shows that this ejected He II feature results in a narrow CME visible in LASCO difference images. Figures 1*d* and 1*f* are respectively LASCO intensity images from before and after the

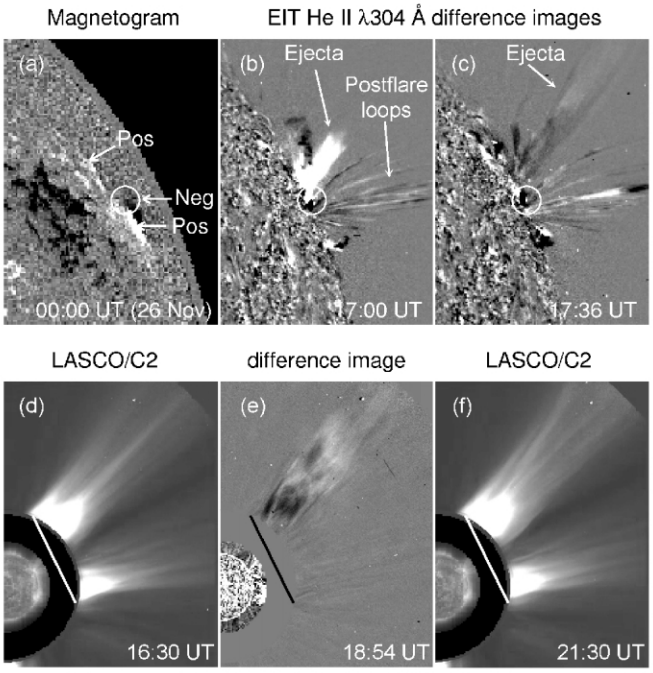

FIG. 1.—(*a*) MDI magnetogram of the eruption source region on the day before limb passage, with the white circle centered on a negative (*black*) polarity region embedded in positive (*white*) polarity (see text). Positive ("Pos") and negative ("Neg") regions, indicated by arrows, can be compared with Fig. 3. (*b*, *c*) Sequence of EIT He II difference images showing the lower atmosphere during one of the eruptions occurring on November 27 (next to a set of preexisting evolving postflare loops, from a large-scale CME on the previous day, unrelated to our events). Images are on the same scale as (*a*) and registered with (*a*) in the north-south direction. The circle is from (*a*) and shows the location of embedded polarity at the limb. (*e*) LASCO C2 difference image showing the consequent streamer puff crossing the coronagraph's field of view. (*d*, *f*) Nondifferenced LASCO images of the corona before and after the eruption, showing that the coronal streamer in which the eruption occurs is largely unaffected by the event. The bars in (*d*)–(*f*) show the location of the UVCS slit.

time of the narrow CME, showing that the overall streamer structure was largely unchanged by the passage of the narrow CME. This is one of our stronger streamer puffs: the outward-moving bright structure is similar to larger CMEs and suggests a plasmoid-type magnetic structure.

Our ejections were homologous in He II, occurring at a rate of about six to eight per day, and emanated from (or at least involved) the same mixed-polarity region marked in Figure 1*a*. Table 1 gives kinematic parameters we derived from the EIT He II ejections, and information on concurrent *GOES* soft X-ray bursts (we do not know with certainty the source of the *GOES* events, but from the close time correspondence our events are likely candidates).

UVCS observations covered November 26, 18:39 UT, to November 29, 02:56 UT, with four data gaps. The UVCS slit was 27″ wide and was centered on and oriented normal to the solar radius 27° north in the west quadrant, at 1.7 $R_\odot$ from disk center (Fig. 1). Spectra were acquired (with a time resolution of 120 s) over several wavelength intervals including lines from both cool ions (e.g., C III and O VI, with peak formation temperatures T_{peak} of, respectively, $10^{4.8}$ and $10^{5.5}$ K), and hot ions (e.g., Fe X, Si XII, and Fe XVIII, with, respectively, T_{peak} of $10^{6.0}$, $10^{6.3}$, and $10^{6.7}$ K). Figure 2 (*top*) shows that during the observations there are several sudden, strong bright C III events. The first five of these are during the EIT He II interval and correspond closely to the He II ejections. These features appear in UVCS at a location and times consistent with the expected arrival location and times of the He II ejections according to estimates made using the θ, t_{st}(EIT) and v_{le}(EIT) values of Table 1. These consistencies make the association of the UVCS events with the He II eruptions unambiguous. Because the bright C III events are well above the stray-light contamination at 1.7 $R_\odot$ and the C III ion has too low a T_{peak} to show up in coronal spectra, the UVCS data suggest that the ejections consist primarily of cool material ($T \sim 6 \times 10^5$ K), as confirmed by the absence of corresponding emission in the Fe X λ1028.0, Si XII λλ499.4, 520.7, or Fe XVIII λ974.8 lines.

Table 1 also gives kinematic parameters derived from UVCS data. The inclination angle, α, from the plane of the sky was derived from Doppler-shifted line profiles by estimating the velocity component v_{los} along the line of sight. To this end, since there was no reference C III background coronal emission, and the ejections also gave rise to brightenings in the O VI λλ1032, 1037 doublet (spatially coincident with those observed in the C III line), we resort to these lines to determine v_{los}. We first determined v_{los} by fitting a Gaussian to the O VI line profile derived by subtracting the average coronal profile before the ejection arrival from the following exposures. This allowed us to derive, from the v_{le}(EIT/UV) values, an estimate for α. All the ejections were redshifted in the UVCS spectra, indicating that the ejecta moved westward (i.e., away from the observer, $\alpha > 0$) from the source region. Moreover, many ejections showed in EIT images a strong inclination with respect to the projected radial from the Sun ($\theta > 0$; see, e.g., Figs. 1*b* and 1*c*) northward from the source region.

The bottom panel of Figure 2 shows results from LASCO observations; the strong event beginning near 20 UT on November 26 is related to a large-scale CME eruption from near 17 UT on the same day and is not the type of narrow CME represented in Figure 1. The four strongest LASCO events between about 16:00 UT on the 27th and the end of the plot are all narrow CMEs. At least two episodes, one consisting of UVCS events 7 and 8 and the other UVCS event 11, extend through UVCS and both LASCO coronagraphs. For other strong LASCO episodes, such as that beginning near 17:00 UT on the 27th (which is the event of Fig. 1) and the episode beginning near 16:15 UT on the 28th, disturbances are obvious in both coronagraphs but occur during UVCS data gaps; these strong events are all "plasmoid-type" puffs. Some UVCS events (e.g., UVCS events 5, 12, 15, and 16) are associated with only weak LASCO events ("gusts"), while UVCS events 3, 4, and 9 result in virtually no LASCO event at all.

3. THE MECHANISM

Our observations indicate that virtually all the ejections from the compact site reach at least UVCS heliocentric distances (1.7 $R_\odot$), but only some of these escape as strong plasmoid-type streamer puffs, while others are apparently trapped below LASCO C2 heliocentric distances (2 $R_\odot$) and result in weak gust-type streamer puffs or no detectable puff at all. We now present a possible scenario to explain these properties.

Figure 3*a* gives the pre-eruption magnetic configuration that we draw based on the observed field and the LASCO white-light streamer configuration. Wedged inside the southern edge of the streamer base is the compact bipole at the northern edge of the sunspot (Fig. 1*a*); the positive polarity of this bipole is against or inside of the main positive spot. North of the negative portion of the bipole is weaker positive flux. Much farther

TABLE 1

EJECTA OBSERVED BY EIT (He II) AND UVCS (C III): KINEMATIC PARAMETERS AND CORRESPONDENCE WITH *GOES* X-RAY BURSTS AND LASCO STREAMER PUFFS

He II Event[a]	C III Event[b]	t_{st}(EIT)[c] (UT)	v_{le}(EIT)[d] (km s^{-1})	θ[e] (deg)	t_{st}(UVCS)[f] (UT)	v_{le}(EIT/UV)[g] (km s^{-1})	α[h] (deg)	*GOES* Burst?[i]	Puff?[j]
1	1	17:42 ± 6	…	25 ± 5	18:46 ± 4	130 ± 20	75 ± 5	No	[k]
2a	…	18:30 ± 6	…	…	…	…	…	Yes, C3	[k]
2b	2	18:42 ± 6	>130	15 ± 5	19:32 ± 4	170 ± 35	4 ± 2	Yes, C3	[k]
3	[l]	04:30 ± 6	140 ± 40	30 ± 5	…	…	…	?[m]	No
4	3	07:12 ± 24	160 ± 60	?[n]	07:51 ± 4	>120	<50	Yes, B1	No
5	4	13:12 ± 24	>90	20 ± 10	14:18 ± 4	150 ± 65	~0	Yes, B1	No
6	[l]	16:42 ± 6	180 ± 60	25 ± 5	…	…	…	Yes, C4	Yes
7a	5a	21:01 ± 12	180 ± 60	20 ± 5	21:44 ± 4	220 ± 80	50 ± 15	Yes, C3	Yes[o]
…	5b	[p]	…	…	21:46 ± 4	…	…	Yes, C3	Yes[o]
7b	5c	21:30 ± 6	>130	30 ± 5	22:14 ± 4	195 ± 45	4 ± 2	Yes, C3	Yes[o]

[a] Sequential identification of events seen in He II.
[b] Sequential identification of events seen in C III; differs from numbers in the previous column because not all events are seen in both instruments.
[c] Estimate of ejection start in He II. Uncertainties (in minutes) are determined by the EIT time cadence.
[d] Velocity estimate from EIT images. Uncertainties are due to EIT cadence and to visual estimates of ejection front in images.
[e] Approximate inclination from vertical at solar surface of ejection early in its evolution.
[f] Time of first sighting in UVCS.
[g] Velocity estimate based on t_{st}(EIT) and t_{st}(UVCS).
[h] Ejection inclination along the line of sight (see text). Positive is away from the observer.
[i] Background-subtracted *GOES* levels are indicated.
[j] "Yes" indicates a discernible streamer puff in the LASCO C2 running-difference movie.
[k] Cannot be determined, because of overlap with the CME event of 26 November, 17 UT.
[l] Occurred during UVCS data gap.
[m] Obscured by elevated *GOES* flux.
[n] Eruption start not seen well enough to estimate this quantity.
[p] Seen in UVCS only; possibly unresolved in EIT because of insufficient cadence.
[o] Entries refer to a single streamer puff.

north, in the polar crown region, is negative flux that closes the streamer arcade on its north side. From south to north, then, the polarities are positive, negative, positive, and negative, and these are reflected in the polarities labeled in Figure 3*a* (arrows in Fig. 1*a* point to the first three of these polarities in the data, while the northernmost negative region is beyond the field of view); this illustration also assumes that a flux rope has already formed above the southernmost neutral line. The streamer's main neutral line is between the northernmost large-area negative and positive polarities, far removed from the source of our puffs.

Figure 3*b* shows the early phase of the production of a plasmoid puff. A core-field eruption occurs along the magnetic neutral line of the bipole (as in typical eruptive flares; see, e.g.,

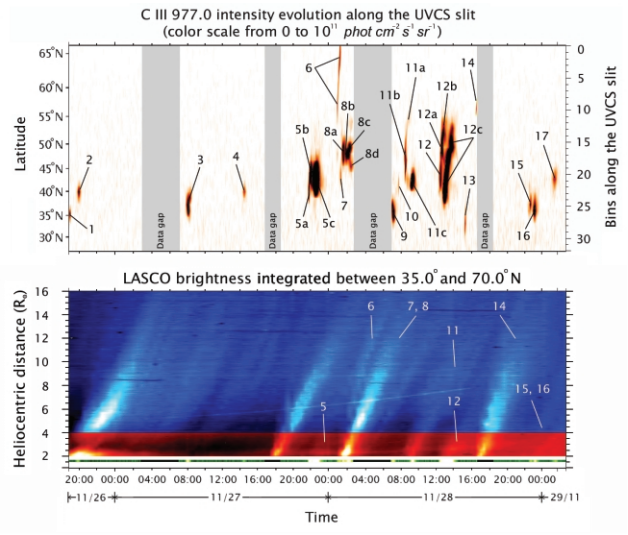

FIG. 2.—*Top*: UVCS C III λ977 line intensity events in time and latitude. *Bottom*: Time-distance evolution of the LASCO C2 (from 2 to 4 $R_\odot$) and C3 (from 4 to 16 $R_\odot$) white-light intensity, integrated between latitudes N35° and N70°. The average intensity at a time preceding the first event has been subtracted from all images. The thin horizontal band at 1.7 $R_\odot$ shows the C III λ977 intensity integrated along the UVCS slit and the UVCS data gaps (*black intervals*). In both panels, events are labeled by their UVCS number (see Table 1).

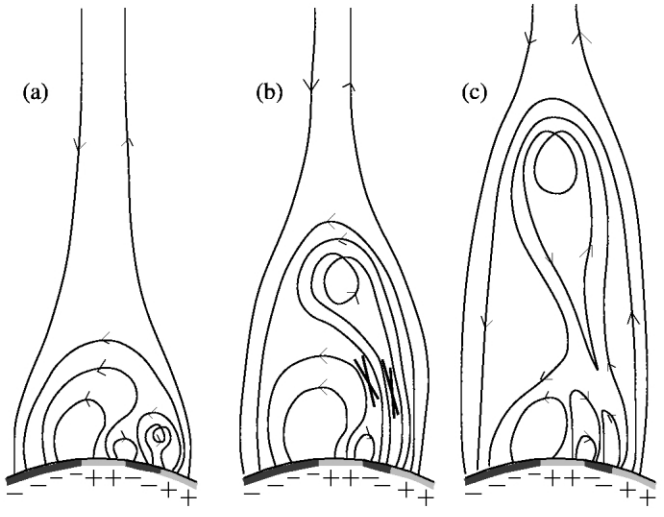

FIG. 3.—Two-dimensional illustration of a twisted core magnetic field exploding and reconnecting to produce a plasmoid-type streamer puff. (*a*) Pre-eruption configuration. Dark and light bands at the base in each sketch respectively represent negative and positive polarities. South is to the right and north is to the left, and all but the leftmost negative polarity correspond to the arrows in Fig. 1*a*. (*b*) Eruption of the core field from the included-polarity region, and resulting reconnections (*elongated crosses*). (*c*) These reconnections unleash a plasmoid that becomes the core of the streamer puff. After the ejection, the initial configuration is restored.

Moore et al. 2001), resulting in an expulsion of the bipole field up a loop of the streamer arcade. The exploding core field reconnects in its interior ("internal reconnection"), producing flare emissions low in the atmosphere. This emission is faint at best in EIT Fe XII images, presumably because it is weak and of short duration. But the *GOES* bursts (Table 1) indicate that these explosions are flares, and surges are often associated with compact flares (see, e.g., Shibata 2001). In addition to the internal reconnection, "external reconnection" will occur between the exploding bipole field and the arcade field of opposite polarity on the north side of the exploding bipole, as in Figure 3*b*. The external and internal reconnections result in the configuration of Figure 3*c*, where the central part of the exploding field has become largely disconnected from the photosphere and moves out along the streamer, creating the streamer puff. Since the exploding region is compact, only a small portion (a loop) of the streamer arcade will be blown out with the ejection, leaving the large bulk of the streamer arcade and streamer intact. After the ejection, the lower fields reconnect, essentially reinstating the configuration of Figure 3*a*, which allows for a repetition of the eruptions in the homologous sequence (cf. Sterling et al. 2001).

Plasmoid ejections that do not have enough energy to break through the closed arcade portion of the streamer or to strongly inflate the loop top result in no streamer-puff CME. The nonplasmoid puffs (gusts) could result from an upward bumping of the streamer by the ejection, expanding the streamer-arcade loop but not blowing it open, thereby generating a pulse or gust of solar wind that travels outward along the open streamer field.

Another possibility is that some of the core-field eruptions do not explode the compact bipole far up the leg of the arcade loop but only cause it to inflate somewhat and reconnect with one side of the loop foot; this external reconnection would be like that in Figure 3*b*, but much lower in the leg of the arcade loop. This reconnection could lead to ejections resulting in plugs of gas or jetlike structures (see, e.g., Sterling et al. 1991, 1993; Shibata 2001). He II events 2 and 7 may result from this or a similar process, as they have wider bases and a more jetlike appearance than most of the other events.

4. DISCUSSION

In the past, narrow CMEs have been studied by Gilbert et al. (2001) and Dobrzycka et al. (2003). Different from our events, only one of the Gilbert et al. events was streamer related. Their events were not homologous, and most of them emanated from a "sharp bend" in a magnetic neutral line: beyond this, little is known of their events' source regions. Because several of the Gilbert et al. events were related to filaments, it could be that some of their narrow CMEs are small-scale versions of the "standard model" for solar eruptions, whereby a highly sheared core field along the main neutral line of an arcade erupts and carries the field surrounding it out into the heliosphere as a CME. From Figure 2 (*bottom*), we estimate the velocities of our three strongest narrow CMEs to be 300 ± 50 km s^{-1}, which is comparable to Gilbert et al.'s velocity estimate for "unstructured" events (359 ± 148 km s^{-1}), although their "structured" events had higher velocities (473 ± 58 km s^{-1}). It is unclear whether there is any correspondence between their two classes of narrow CMEs and any of our events.

Dobrzycka et al. (2003) observed five of the Gilbert et al. events with UVCS, primarily in H I Lyα and O VI $\lambda\lambda$1032, 1037. Formation temperatures for these lines range over about $(0.5–1.5) \times 10^6$ K, substantially hotter than the ≈60,000 K C III line. Dobrzycka et al. report C III data only for the 1999 March 27 event; they found that the line intensity was weak, implying that it either did not contain as much cool material as ours or underwent a larger Doppler dimming. Also, Dobrzycka et al. (2003) did not find any significant line Doppler shift (and hence no significant inclination α with respect to the radial direction, in the case of near-limb events) for the ejected plasma in UVCS spectra for their events, whereas we find a high inclination for some of our events.

Recently, Ko et al. (2005) studied a near-limb coronal jet that occurred in step with a faint, narrow CME. Their jet and faint CME may respectively be similar to our He II ejections and gust-type streamer puffs. However, Ko et al. argue that the jet and CME were not related and that eventually the jet plasma comes back to the solar surface.

We summarize the main differences between the streamer puffs reported here and the narrow and/or typical CMEs previously studied: Streamer puffs (1) occur recursively inside a coronal streamer whereas nearly all previous observations of narrow CMEs report only single events not associated with coronal structures; (2) do not blow out the entire streamer (as in typical CMEs), although plasma escapes into the solar wind as a plasmoid or gust along the streamer; (3) originate from nonradial ejecta from compact ejective flares; and (4) are produced in a different way than has been recognized in previous studies of narrow CMEs (as shown in § 3).

A. C. S. and R. L. M. were supported by NASA's Office of Space Science Supporting Research and Technology and Sun-Earth Connection Guest Investigator programs. A. B. and G. P. acknowledge support from ASI-INAF contract I/035/05/0 to the Observatory of Turin. *SOHO* is a mission of international cooperation between ESA and NASA.

REFERENCES

Brueckner, G. E., et al. 1995, Sol. Phys., 162, 357
Delaboudinière, J.-P., et al. 1995, Sol. Phys., 162, 291
Dobrzycka, D., Raymond, J. C., Biesecker, D. A., Li, J., & Ciaravella, A. 2003, ApJ, 588, 586
Gilbert, H. R., Serex, E. C., Holzer, T. E., MacQueen, R. M., & McIntosh, P. S. 2001, ApJ, 550, 1093
Ko, Y.-K., et al. 2005, ApJ, 623, 519
Kohl, J. L., et al. 1995, Sol. Phys., 162, 313
Moore, R. L., Sterling, A. C., Hudson, H. S., & Lemen, J. R. 2001, ApJ, 552, 833
Scherrer, P. H., et al. 1995, Sol. Phys., 162, 129
Shibata, K. 2001, in Encyclopedia of Astronomy and Astrophysics, ed. P. Murdin (Bristol: IoP), 3258
St. Cyr, O. C., Burkepile, J. T., Hundhausen, A. J., & Lecinski, A. R. 1999, J. Geophys. Res., 104, 12493
St. Cyr, O. C., et al. 2000, J. Geophys. Res., 105, 18169
Sterling, A. C., Mariska, J. T., Shibata, K., & Suematsu, Y. 1991, ApJ, 381, 313
Sterling, A. C., Moore, R. L., Qiu, J., & Wang, H. 2001, ApJ, 561, 1116
Sterling, A. C., Shibata, K., & Mariska, J. T. 1993, ApJ, 407, 778